

Thermal Decomposition of Ferrocene as a Method for Production of Single-Walled Carbon Nanotubes without Additional Carbon Sources

Amelia Barreiro,^{*,†,‡} Silke Hampel,[†] Mark H. Rummeli,[†] Christian Kramberger,[†] Alexander Grüneis,[†] Kati Biedermann,[†] Albrecht Leonhardt,[†] Thomas Gemming,[†] Bernd Büchner,[†] Adrian Bachtold,[‡] and Thomas Pichler[†]

IFW Dresden, P.O. Box 270116, D-01171 Dresden, Germany, and Institut Català de Nanotecnologia and Centro Nacional Microelectrónica, Campus Universitat Autònoma de Barcelona, E-08193 Bellaterra, Spain

Received: June 12, 2006; In Final Form: August 22, 2006

A new method to grow bulk quantities of single-walled carbon nanotubes (SWCNTs) by a catalytic chemical vapor deposition (CVD) process with the possibility of varying the pressure has been developed and is reported in this paper. Thermal decomposition of ferrocene provides both catalytic particles and carbon sources for SWCNT growth using Ar as a carrier gas. Upon an increase in the pressure, the mean diameter of the SWCNTs decreases. In fact, high abundances of SWCNT with diameters as small as 0.7 nm, which is the limit for stable caps with isolated pentagons, can be obtained. An additional advantage of this method is that as no external carbon sources are required, SWCNT synthesis can be achieved at temperatures as low as 650 °C.

1. Introduction

Since their discovery in 1991 by Iijima,¹ carbon nanotubes (CNTs) have attracted widespread attention. Several methods can be applied for nanotube production, the most popular being arc discharge,² laser ablation,³ and chemical vapor deposition (CVD)⁴ such as the HiPco process.⁵ The unique electrical and mechanical properties of these sp²-hybridized molecular nanostructures make them one of the most promising building blocks for nanoscale science and nanotechnology. Their small size, large aspect ratio, large current carrying density, ballistic transport properties, and exceptional mechanical properties⁶ render CNTs promising candidates for application in nanoelectronics, nanomechanics, and composite materials.⁷ So far, many different nanoscale devices based on CNTs as active elements such as field-emission displays,⁸ ultrastrong yarns,⁹ interconnects,¹⁰ batteries,¹¹ single-molecule transistors,¹² nanobalances,¹³ and nanosensors¹⁴ have been successfully realized. Many of these applications demand very pure, well-defined, and cheap CNTs on a bulk scale. To this end, CVD is in comparison to arc discharge and laser ablation, the best choice because of its upward scalability, low cost, and rather low production temperatures. In particular, lower reaction temperatures¹⁵ are essential for implementing the synthesis of SWCNT into existing and well-established processes in semiconductor industries. Among the available CVD processes, injection CVD and aerosol-assisted (AA) CVD methods are exceptionally cheap and well-suited for scaling up to mass production of CNT with a defined nanotube diameter distribution. These processes have already been widely used for the growth of multiwall CNTs (MWCNT)¹⁶ and have also been successfully applied for the synthesis of SWCNT¹⁷ using ferrocene as a catalyst precursor and ferrocene promoted by sulfur, respectively. Recently, this CVD process has also been applied for the direct spinning of carbon nanotube fibers in a continuous manner.¹⁸ Also, some

other authors have applied similar methods suitable for large-scale production of SWCNTs using ferrocene as a metal precursor for the production of SWCNTs without using sulfur as a promoter.^{19–21} The advantages of using ferrocene as an iron precursor are its innocuity and low cost. In fact, it is difficult to imagine a large-scale production of SWCNT based on a catalyst made from a suspected cancerous agent precursor such as nickelocene.¹⁹ Another process that is very suitable for scaling up nanotube growth to mass production is the HiPco process.⁵ In this paper, we present a method similar to the HiPco process for continuous high-yield production of extremely narrow SWCNT using ferrocene as the sole source for both catalytic Fe particles and carbon feedstock. The feasible control on the reaction parameters renders this technique a stable and reproducible route of synthesis of bulk-scale SWCNTs with defined diameter distribution. As no external carbon sources are required, we show that it is possible to synthesize SWCNTs in a continuous manner at temperatures as low as 650 °C. A further advantage is that ferrocene is not toxic in contrast to Fe(CO)₅ and CO, which are required for the HiPco process.

2. Experimental Procedures

Figure 1 shows a parallel cross-section of the high-pressure reactor used for this process that is similar to the one used for the HiPco process.⁵ This reactor consists of a quartz tube surrounded by an electrical heating element. Both the reactor and the quartz tube are contained within a thick-walled aluminum cylinder. The heating element itself and the space between the quartz tube and the inner wall of the aluminum cylinder reside under an atmosphere of argon maintained at slightly higher pressure than that inside the quartz tube.

A gas mixture consisting of 2000 sccm argon mixed with the sublimated gaseous ferrocene was flowed through the quartz tube. The rate at which the reactant gases were heated had substantial effects on the amount and quality of SWCNTs produced as reported by Nikolaev et al.⁵ Rapid heating of the argon/ferrocene mixture enhanced the formation of nanotubes. The argon carrier gas and the ferrocene were introduced through

* Corresponding author. Tel.: 0034 93 594 77 00; fax: 0034 93 580 14 96; e-mail: a.barreiro@ifw-dresden.de.

[†] IFW Dresden.

[‡] Campus Universitat Autònoma de Barcelona.

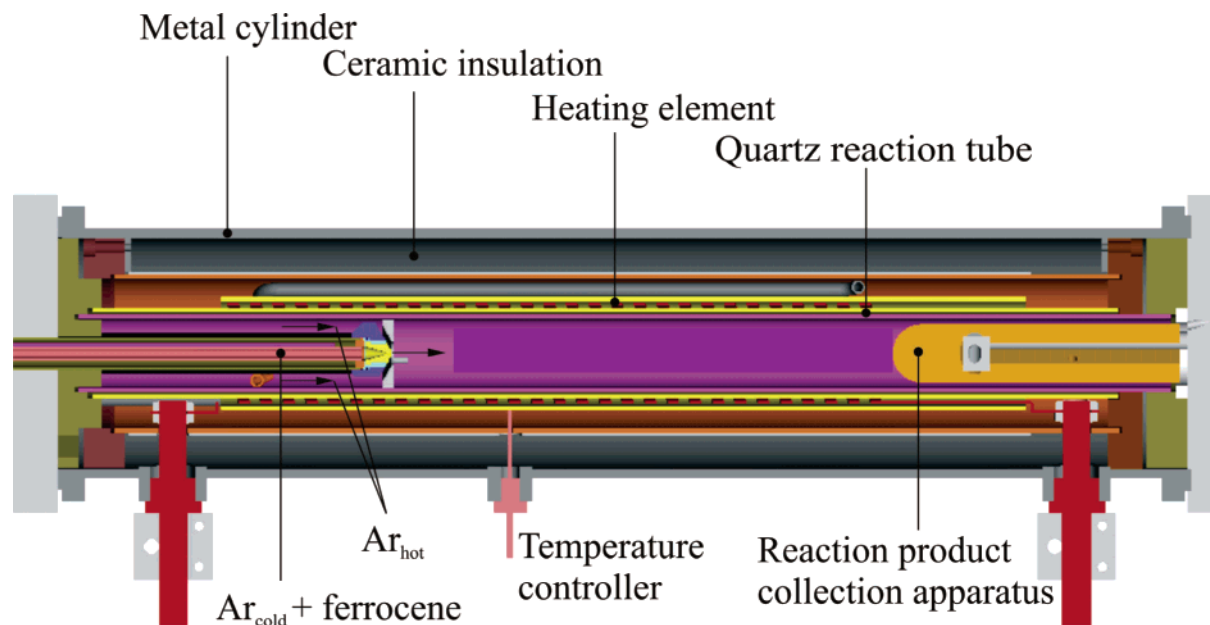


Figure 1. Axial cross-section of the high-pressure CVD reactor used for the SWCNT synthesis via thermal decomposition of ferrocene.

a water-cooled injector tipped with a copper injection nozzle positioned inside the quartz tube, which maintained the gases at low temperatures until they were injected into the furnace, resulting in rapid heating. Around the exit of this injector, a shield with holes was positioned through which preheated argon passed at a 150 sccm flow rate to mix with the flow emerging from the injector, further increasing the heating rate of the injected gas. The preheated argon passed to the reaction zone, where it collided and mixed with the cold injector flow emerging from the copper nozzle, which protruded into the reaction zone. The temperature of the heated argon/ferrocene mixture passing through the injection nozzle could be controlled and was set at 90 °C for all our experiments to avoid the decomposition of ferrocene before entering the reaction chamber. The pressure of the cold argon/ferrocene was held at 2 bar higher than inside the reaction chamber, thus favoring a rapid and vigorous injection. The growth temperature was found to be in the range of 650–900 °C, and the growth pressure was varied from 1 to 5 bar.

The SWCNT was carried out of the reactor by the hot gas flow and into a product collection apparatus. There, the gas flow passed through a series of filters, and the soot containing SWCNTs condensed on a water-cooled copper collector.

The reaction products were characterized using scanning electron microscopy (SEM) (Philips XL30), transmission electron microscopy (TEM) (Tecnai F30 (FEI)), Fourier Transform Raman spectroscopy (FTRS) with a Bruker FT RFS 100/s Raman spectrometer, and optical absorption spectroscopy (OAS) with a Bruker IFS 113V/88 spectrometer.

3. Results and Discussion

At a temperature higher than 500 °C, ferrocene decomposes completely spontaneously following the chemical reaction $\text{Fe}(\text{C}_5\text{H}_5)_2 \rightarrow \text{Fe} + \text{H}_2 + \text{CH}_4 + \text{C}_5\text{H}_6 + \dots$ as well as reactive hydrocarbons.²² Thus, when ferrocene enters the reaction zone, iron clusters and reactive carbon in the gas phase are produced. Upon these clusters, acting as catalyst nuclei, the SWCNTs nucleate and grow with the carbon atoms provided only from the ferrocene.

We first turn to a local-scale analysis of the sample morphology and structure using both SEM and TEM. In the SEM

micrograph in Figure 2, the morphology of a sample grown at 1 bar and 900 °C is shown and can be considered as typical. One can see the overall sample morphology that consists of a high amount of spaghetti-like bundles of carbon nanotubes that are rather long.

Direct evidence for the growth of SWCNT is given by TEM. Predominantly, the samples consisted of long bundles of straight SWCNTs decorated with low amounts of amorphous species, carbon-coated iron clusters, and individual SWCNTs. Despite extensive TEM studies on various samples synthesized between 650 and 900 °C and 1 bar and 5 bar, only exiguous amounts of double-walled or multi-walled carbon nanotubes were observed. Thus, this synthesis process is very selective toward SWCNT. Most of the SWCNTs form bundles with a diameter between 20 and 30 nm, although some isolated SWCNT could be detected. The diameters of the observed individual SWCNT range from 0.7 to 1.7 nm. Typical diameters of the bundles are 20 nm–30 nm. Figure 3 depicts two TEM micrographs of SWCNT synthesized at 900 °C and 1 bar. These results are very similar independent of the reaction conditions, and hence, the micrographs depicted in Figure 3 can be denoted as typical.

However, as TEM gives only a local probe for the estimation of the yield, relative defect concentration, diameter, and diameter distribution, we further characterized our samples optically with bulk-scale measurements. Raman spectroscopy, in this case FTRS, is a powerful tool to analyze SWCNT. The Raman spectrum of SWCNTs shows three responses of major interest. The so-called G-line (graphitic line) is located around 1600 cm^{-1} . This feature is common to all sp^2 -hybridized carbon. Around 1300 cm^{-1} , there is the D-line (defect line). This line is due to a second-order Raman process only possible via the scattering on a defect in the SWCNT.²³ Finally, there is the radial breathing mode (RBM), which allows the diameters of the nanotubes to be evaluated from the resonantly enhanced nanotubes by the well-established inverse diameter dependence of the RBM $\delta\nu = (234 \text{ cm}^{-1}/d + 14 \text{ cm}^{-1})$.²⁴ Typical Raman spectra of samples synthesized at 900 and 650 °C are depicted in Figure 4 upper spectrum and lower spectrum, respectively. There are no significant changes in the Raman spectra, neither in the D-line to G-line ratio nor a shift in the RBM when increasing the reaction pressure up to 5 bar, and the spectra

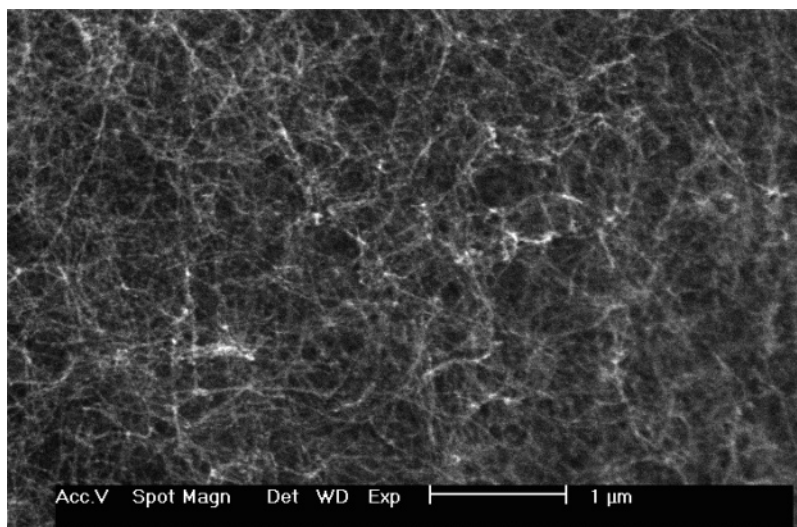


Figure 2. SEM micrograph showing the morphology of as-grown SWCNT at 900 °C and 1 bar.

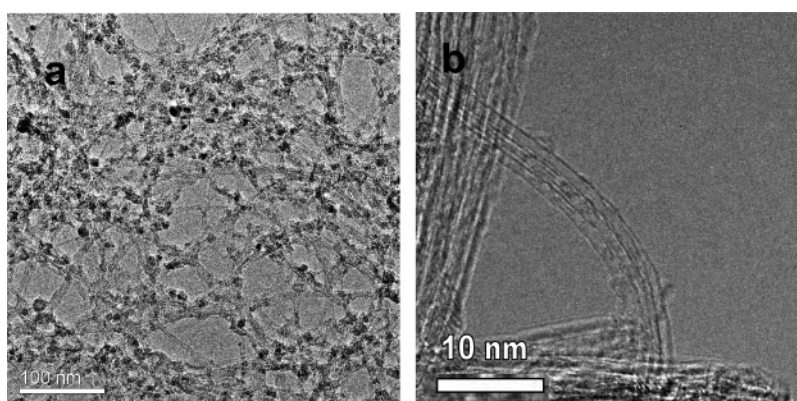


Figure 3. Overview (a) and high magnification (b) of pristine SWCNT produced at 900 °C and 1 bar.

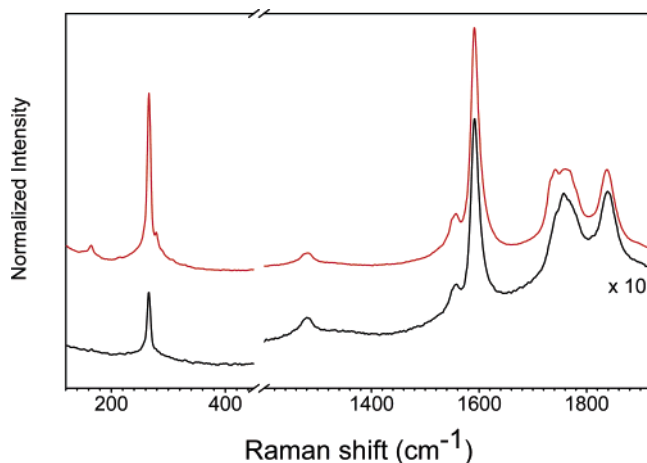


Figure 4. Typical Raman spectrum of a sample synthesized at temperatures of 900 °C (upper spectrum) and 650 °C (lower spectrum).

show a defined peak at 270 cm^{-1} corresponding to 0.9 nm diameter SWCNT. This is very similar to standard HiPco material and a first hint that the relative yield of thick diameter tubes, such as the ones with 1.4 nm thickness (small RBM in the upper spectrum in Figure 4 at about 164 cm^{-1}) is much smaller as in most of the other CVD processes or for SWCNT produced via laser ablation and arc discharge, which have a similar resonance Raman cross-section following the Kataura plot.²⁵ One should note that Raman spectroscopy with one single laser line is not susceptible to fine changes in mean diameter.

This is because only a certain subset of the nanotubes can couple to that one laser line, following the Kataura plot.²⁵ This is even more so for infrared excitations and such narrow SWCNTs.

The Raman spectra of samples synthesized in the temperature range from 750 to 900 °C are very similar. For low-temperature SWCNT synthesis below 700 °C, there is a decrease in the yield as can be seen if comparing the two spectra in Figure 4 due to, on one hand, a decrease of the height of the RBM. On the other hand, this can also be related to a change in the SWCNT diameter distribution. Nevertheless, the overall SWCNT yield can be estimated from the relative Raman signal of the G-lines under the assumption of a sample density independent from the synthesis temperature and a sample thickness bigger than the penetration depth of the laser light. Both conditions are fulfilled for these samples, and we observe a reduction of the SWCNT yield by a factor of 10 when reducing the synthesis temperature from 750 to 650 °C. Furthermore, the relative defect concentration in the samples can be analyzed in a nondestructive way from the ratio between the G-line and the D-line. As can be seen in the upper spectrum in Figure 4, the D/G ratio in all our samples grown at temperatures above 750 °C is below 0.1 while for temperatures below 700 °C is usually around 0.25. A comparison of these values to other contemporary scalable routes of synthesis (e.g., AA CVD of MWCNT¹⁶ with a typical D/G ratio around 0.5) clearly highlights the benefits of the synthesis method reported in this paper.

For a detailed analysis of mean diameters and diameter distribution in a bulk sensitive way, we utilize OAS. OAS has been proven to be a powerful tool to evaluate these prop-

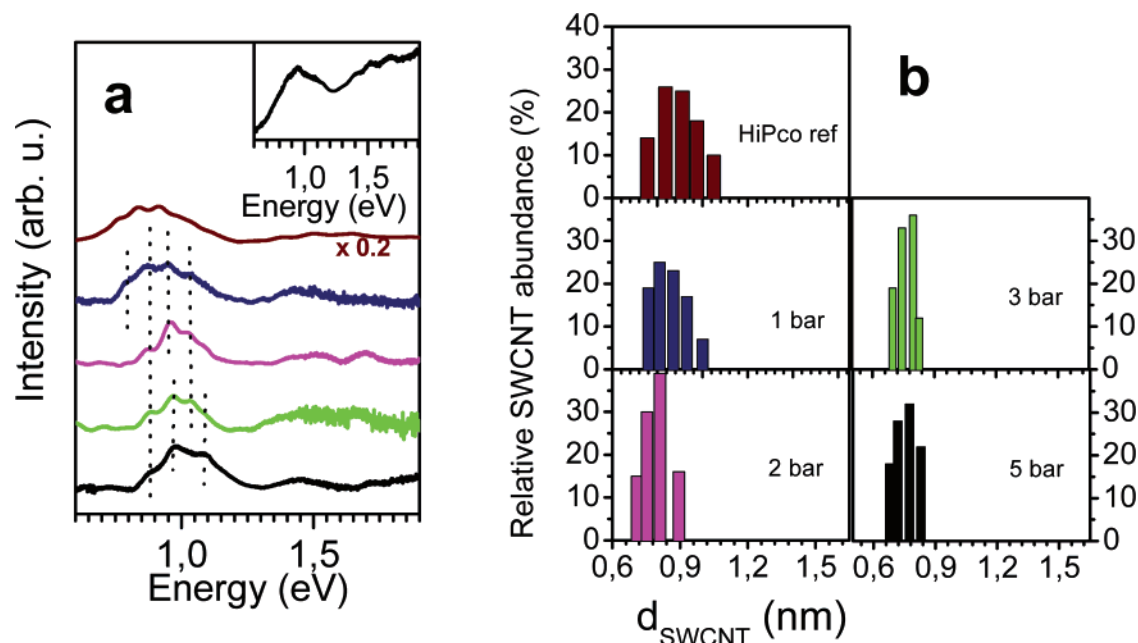


Figure 5. (a) OAS results with typical spectra synthesized at 900 °C and 5, 3, 2, and 1 bar from bottom to top along with a decreasing mean diameter distribution with increasing pressure and in comparison to purified HiPco material⁵ (spectrum at the top). For clarity and a better comparison, the relative peak intensity is divided by five for this curve. The dotted lines guide the eye to the signature of preferential growth of SWCNT with diameters of 0.95, 0.87, 0.81, 0.79, 0.74, and 0.70 nm from left to right. The inset shows a typical unstrapped spectrum (900 °C, 3 bar). (b) Diameter distribution as evaluated from the corresponding spectra on the left for the HiPco reference material and for the SWCNTs produced by thermal decomposition of ferrocene at 1, 2, 3, and 5 bar.

erties.^{17,26–28} For the determination of the mean diameter, there is a well-established relation $E_{11}^S = 2 - \gamma_0 a_0/d - \Delta$, where E_{11}^S is the center of the first absorption peak, $\gamma_0 = 2.9$ eV is the tight binding overlap integral, a_0 is the C–C distance of 0.142 nm, and $\Delta = 90$ meV is an excitonic correction for bundled SWCNT.²⁶ Besides detailed information on the diameter distribution, OAS is also suitable for determining the total yield of SWCNT with respect to amorphous impurities by taking into account the linear background with respect to peak intensities.^{17,26–29} OAS spectra of SWCNT material synthesized at pressures of 1, 2, 3, and 5 bar and 900 °C as well as a reference spectrum of purified HiPco material are depicted in Figure 5a. The inset shows the unstrapped spectrum of SWCNTs synthesized at 3 bar. As compared to the purified HiPco material, the relative yield of all our pristine samples is about 20% as we assume all the samples to expose fairly similar densities. In this context, we point out that, similar to what has been observed previously for SWCNT raw material with different qualities,²⁹ the purification behavior crucially depends on the relative amount of amorphous carbon and catalyst particles. For our ferrocene SWCNTs, we find that the purification parameters using selective oxidation in air plus HCl treatment to remove the Fe catalysts, which we are currently optimizing, strongly differ from standard HiPco material.

After evaluating the OAS data, it can be stated that the majority of the investigated SWCNTs have diameters between 0.7 and 1.1 nm, and the abundance of bigger diameter SWCNTs is fairly low. The gradual shift of the absorption peak upon increasing pressure indicates a decrease in mean diameter. From a root-mean-square fit, the mean diameter of the SWCNT changes from 0.84 nm (1 bar) to 0.8 nm (2 bar), 0.78 nm (3 bar), and 0.75 nm (5 bar). The dotted vertical lines in Figure 5a guide the eye to the fine structure in the first OAS peak. These lines point to a preferential growth of SWCNT with distinct diameters of 0.95, 0.87, 0.81, 0.79, 0.74, and 0.70 nm, respectively.

A detailed analysis of the diameter distributions is depicted in Figure 5b. The compilation of the purified HiPco reference material and the SWCNTs synthesized at 900 °C and at 1, 2, 3, and 5 bar clearly demonstrates how the reaction pressure can be used to fine-tune the mean diameter. This CVD technique bears some similarities to laser evaporation. Thus, the growth and nucleation of the SWCNT may occur through a similar mechanism as described in ref 28. Indeed, fullerene capping in the nucleation step could account for the selective bulk synthesis of extremely narrow SWCNTs and the observed preferential growth that is indicated by the dashed lines in Figure 5a. Interestingly, the smallest observed diameter is by far not the least abundant at 5 bar reaction pressure. There seems to be a hard limit for the synthesis of diameters less than 0.7 nm. This matches quite closely to the diameter of C₆₀, which is the smallest fullerene that can satisfy the isolated pentagon rule, and is expected to be the hard limit for any bundled or isolated SWCNTs.

4. Conclusion

The high-pressure ferrocene method is suitable for the large-scale synthesis of high quality and extremely narrow SWCNTs. The majority of the obtained diameters are in the range of 0.7–1.1 nm. The mean diameter can be tailored by varying the reaction pressure. Higher pressures lead to smaller diameters. The diameters are strictly limited by the isolated pentagon rule, which is needed to form a stable cap for SWCNT nucleation.

Acknowledgment. The authors thank D. Selbmann for valuable scientific work; G. Kreutzer, S. Pichl, and R. Schönfelder for technical support; and R. Smalley for the delivery of HiPco SWCNTs. M.H.R. and T.P. acknowledge the DFG Projects PI 440/1 and PI 440/3. C.K. acknowledges a fellowship from the International Max Planck Research School. A.G. acknowledges a Schrödinger fellowship J2493 from the Fonds zur Förderung der wissenschaftlichen Forschung (FWF).

References and Notes

- (1) Iijima, S.; Ichihashi, T. *Nature* **1993**, *364*, 603.
- (2) Ebessen, T. W.; Ajayan, P. M. *Nature* **1992**, *358*, 220.
- (3) Thess A.; Lee, R.; Nikolaev, P.; Dai, H.; Petit, P.; Robert, J.; Xu, C.; Lee, Y. H.; Kim, G. S.; Rinzler, A. G.; Colbert, D. T.; Scuseria, G.; Tomanek, D.; Fischer, J. E.; Smalley, R. E. *Science* **1996**, *273*, 483.
- (4) José-Yacamán, M.; Miki-Yoshida, M.; Rendón, L.; Santiesteban, J. G. *Appl. Phys. Lett.* **1993**, *62*, 657.
- (5) Nikolaev, P.; Bronikowski, M. J.; Bradley, R. K.; Rohmund, F.; Colbert, D. T.; Smith, K. A.; Smalley, R. E. *Chem. Phys. Lett.* **1999**, *313*, 91.
- (6) Saito, R.; Dresselhaus, G.; Dresselhaus, M. S. *Physical Properties of Carbon Nanotubes*; Imperial College Press: London, 1998.
- (7) Thostenson, E. T.; Ren, Z.; Chou, T.-W. *Compos. Sci. Technol.* **2001**, *61*, 1899.
- (8) Choi, W. B.; Chung, D. S.; Kang, J. H.; Kim, H. Y.; Jin, Y. W.; Han, I. T.; Lee, Y. H.; Jung, J. E.; Lee, N. S.; Park, G. S.; Kim, J. M. *Appl. Phys. Lett.* **1999**, *75*, 3129.
- (9) Mei, Z.; Atkinson, K. R.; Baughman, R. H. *Science* **2004**, *306*, 1358.
- (10) Kong, J.; Soh, H. T.; Cassell, A. M.; Quate, C. F.; Dai, H. *Nature* **1998**, *395*, 878.
- (11) Gao, B.; Bower, C.; Lorentzen, J. D.; Fleming, L.; Kleinhammes, A.; Tang, X. P.; McNeil, L. E.; Wu, Y.; Zhou, O. *Chem. Phys. Lett.* **2000**, *327*, 69.
- (12) Tans, S. J.; Verschueren, A. R. M.; Dekker, C. *Nature* **1998**, *393*, 49.
- (13) Poncharal, P.; Wang, Z. L.; Ugarte, D.; de Heer, W. A. *Science* **1999**, *283*, 1513.
- (14) Kong, J.; Dai, H. *Science* **2000**, *287*, 622.
- (15) Grüneis, A.; Kramberger, C.; Grimm, D.; Gemming, T.; Rümmeli, M. H.; Barreiro, A.; Ayala, P.; Pichler, T.; Schaman, C.; Kuzmany, H.; Schumann, J.; Büchner, B. *Chem. Phys. Lett.* **2006**, *425*, 301.
- (16) Barreiro, A.; Selbmann, D.; Pichler, T.; Biedermann, K.; Rümmeli, M. H.; Schwalke, U.; Büchner, B. *Appl. Phys. A* **2006**, *82*, 719.
- (17) Barreiro, A.; Kramberger, C.; Rümmeli, M. H.; Grüneis, A.; Grimm, D.; Hampel, S.; Gemming, T.; Büchner, B.; Bachtold, A.; Pichler, T. *Carbon* **2006**; DOI 10.1016/j.carbon.2006.08.013.
- (18) Li, Y. L.; Kinloch, I. A.; Windle, A. H. *Science* **2004**, *304*, 276.
- (19) Smiljanic, O.; Stansfield, B. L.; Dodelet, J.-P.; Serventi, A.; Désilets, S. *Chem. Phys. Lett.* **2002**, *356*, 189.
- (20) Biró, L. P.; Horváth, Z. E.; Koós, A. A.; Osváth, Z.; Vértesy, Z.; Darabont, A. L.; Kertész, K.; Neamtu, C. C.; Sárkozi, Z.; Tapasztó, L. L. *J. Opt. Adv. Mater.* **2003**, *5*, 661.
- (21) Lupo, F.; Rodríguez-Manzo, J. A.; Zamudio, A.; Elías, A. L.; Kim, Y. A.; Hayashi, T.; Muramatsu, M.; Kamalakaran, R.; Terrones, H.; Endo, M.; Rühle, M.; Terrones, M. *Chem. Phys. Lett.* **2005**, *410*, 384.
- (22) Leonhardt, A.; Hampel, S.; Müller, C.; Mönch, I.; Koseva, R.; Ritschel, M.; Elefant, D.; Biedermann, K.; Büchner, B. Chemical vapor deposition. **2006**, *12*, 380.
- (23) Zólyomi, V.; Kürti, J. *Phys. Rev. B* **2002**, *66*, 073418.
- (24) Kramberger, C.; Pfeiffer, R.; Kuzmany, H.; Zólyomi, V.; Kürti, J. *Phys. Rev. B* **2003**, *68*, 235404.
- (25) Kataura, H.; Kumazawa, Y.; Umez, I.; Suzuki, S.; Ohtsuka, Y.; Achiba, Y. *Synth. Met.* **1999**, *103*, 2555.
- (26) Liu, X.; Pichler, T.; Knupfer, M.; Golden, M. S.; Fink, J.; Kataura, H.; Achiba, Y. *Phys. Rev. B* **2002**, *66*, 45411.
- (27) Jost, O.; Gorbunov, A. A.; Pompe, W.; Pichler, T.; Friedlein, R.; Knupfer, M.; Reibold, M.; Bauer, H. D.; Dunsch, L.; Golden, M. S.; Fink, J. *Appl. Phys. Lett.* **1999**, *75*, 2217.
- (28) Rümmeli, M. H.; Borowiak-Palen, E.; Gemming, T.; Pichler, T.; Knupfer, M.; Kalbac, M.; Dunsch, L.; Jost, O.; Pompe, W.; Silva, R.; Büchner, B. *Nano Lett.* **2005**, *5*, 1209.
- (29) Itkis, M. E.; Perea, D. E.; Jung, R.; Niyogi S.; Haddon R. C. *J. Am. Chem. Soc.* **2005**, *127*, 3440.